MAXIMUM PRINCIPLE PRESERVING EXPONENTIAL TIME DIFFERENCING SCHEMES FOR THE NONLOCAL ALLEN–CAHN EQUATION[*]

QIANG DU[†], LILI JU[‡], XIAO LI[§], AND ZHONGHUA QIAO[¶]

Abstract. The nonlocal Allen–Cahn equation, a generalization of the classic Allen–Cahn equation by replacing the Laplacian with a parameterized nonlocal diffusion operator, satisfies the maximum principle as its local counterpart. In this paper, we develop and analyze first and second order exponential time differencing schemes for solving the nonlocal Allen–Cahn equation, which preserve the discrete maximum principle unconditionally. The fully discrete numerical schemes are obtained by applying the stabilized exponential time differencing approximations for time integration with quadrature-based finite difference discretization in space. We derive their respective optimal maximum-norm error estimates and further show that the proposed schemes are asymptotically compatible, i.e., the approximating solutions always converge to the classic Allen–Cahn solution when the horizon, the spatial mesh size, and the time step size go to zero. We also prove that the schemes are energy stable in the discrete sense. Various experiments are performed to verify these theoretical results and to investigate numerically the relation between the discontinuities and the nonlocal parameters.

Key words. nonlocal Allen–Cahn equation, discrete maximum principle, exponential time differencing, asymptotic compatibility, energy stability

AMS subject classifications. 65M12, 65M15, 65R20, 35Q99

DOI. 10.1137/18M118236X

1. Introduction. In this paper, we consider numerical solution of the initial-boundary-value problem of the nonlocal Allen–Cahn (NAC) equation as follows:

$$\text{(1.1a)} \qquad u_t - \varepsilon^2 \mathcal{L}_\delta u + u^3 - u = 0, \qquad \boldsymbol{x} \in \Omega,\ t \in (0, T],$$

$$\text{(1.1b)} \qquad u(\cdot, t) \text{ is } \Omega\text{-periodic}, \qquad t \in [0, T],$$

$$\text{(1.1c)} \qquad u(\boldsymbol{x}, 0) = u_0(\boldsymbol{x}), \qquad \boldsymbol{x} \in \overline{\Omega},$$

where $u(\boldsymbol{x}, t)$ denotes the unknown function, $\Omega = (0, X)^d$ is a hypercube domain in $\mathbb{R}^d$, $\varepsilon > 0$ is an interfacial parameter, and $\mathcal{L}_\delta$ is a nonlocal operator, parameterized

[†]Department of Applied Physics and Applied Mathematics and Data Science Institute, Columbia University, New York, NY 10027 (qd2125@columbia.edu).

[‡]Department of Mathematics, University of South Carolina, Columbia, SC 29208, and School of Mathematical Sciences, Ocean University of China, Qingdao, Shandong 266100, China (ju@math.sc.edu).

[§]Applied and Computational Mathematics Division, Beijing Computational Science Research Center, Beijing 100193, China. Current address: Department of Mathematics, University of South Carolina, Columbia, SC 29208 (li434@mailbox.sc.edu).

[¶]Department of Applied Mathematics, The Hong Kong Polytechnic University, Hung Hom, Kowloon, Hong Kong (zhonghua.qiao@polyu.edu.hk).

by the positive horizon parameter $\delta > 0$ measuring the range of nonlocal interactions. Assume that $\mathcal{L}_\delta$ is defined by

$$(1.2) \qquad \mathcal{L}_\delta u(\boldsymbol{x}) = \frac{1}{2} \int_{B_\delta(\mathbf{0})} \rho_\delta(|\boldsymbol{s}|)\big(u(\boldsymbol{x}+\boldsymbol{s}) + u(\boldsymbol{x}-\boldsymbol{s}) - 2u(\boldsymbol{x})\big) \, \mathrm{d}\boldsymbol{s}, \qquad \boldsymbol{x} \in \Omega,$$

with $B_\delta(\mathbf{0})$ denoting the ball in $\mathbb{R}^d$ centered at the origin, with radius δ, $\rho_\delta : [0, \delta] \to \mathbb{R}$ being a nonnegative kernel function, and $|\cdot|$ standing for the usual Euclidean norm. To enforce the consistency, as $\delta \to 0$, of the nonlocal operator $\mathcal{L}_\delta$ with the standard Laplacian operator $\mathcal{L}_0 := \Delta$, we further assume the kernel ρ_δ satisfies

$$\int_0^\delta r^{1+d} \rho_\delta(r) \, \mathrm{d}r = \frac{2d}{S_d},$$

with S_d being the area of the unit sphere in $\mathbb{R}^d$, or, equivalently,

$$(1.3) \qquad \int_{B_\delta(\mathbf{0})} |\boldsymbol{s}|^2 \rho_\delta(|\boldsymbol{s}|) \, \mathrm{d}\boldsymbol{s} = 2d.$$

Note that (1.3) also means that the kernel ρ_δ has a finite second order moment. The continuum property of the nonlocal operator $\mathcal{L}_\delta$ gives [10, 11]

$$(1.4) \qquad \max_{\boldsymbol{x} \in \overline{\Omega}} |\mathcal{L}_\delta u(\boldsymbol{x}) - \mathcal{L}_0 u(\boldsymbol{x})| \leq C\delta^2 \|u\|_{C^4} \qquad \forall\, u \in C^4_{\mathrm{per}}(\overline{\Omega}),$$

where $C > 0$ is a constant independent of δ. The local limit of the NAC problem (1.1) is exactly the classic (local) Allen–Cahn (LAC) equation taking the following form:

$$(1.5a) \qquad \varphi_t - \varepsilon^2 \mathcal{L}_0 \varphi + \varphi^3 - \varphi = 0, \qquad \boldsymbol{x} \in \Omega, \ t \in (0, T],$$

$$(1.5b) \qquad \varphi(\cdot, t) \text{ is } \Omega\text{-periodic}, \qquad t \in [0, T],$$

$$(1.5c) \qquad \varphi(\boldsymbol{x}, 0) = \varphi_0(\boldsymbol{x}), \qquad \boldsymbol{x} \in \overline{\Omega}.$$

The LAC equation (1.5) is a well-known phase field model used to describe the motion of antiphase boundaries in crystalline solids [1].

In recent years, nonlocal models involving the nonlocal operator (1.2), such as the NAC equation (1.1), have appeared in a variety of applications ranging from physics and materials science to finance and image processing, for instance, phase transition [4, 19], peridynamics continuum theory [37, 38], image analyses [20, 21], and nonlocal heat conduction [7]. Rigorous mathematical analysis of nonlocal models can be found in the literature, e.g., [3, 4, 16], and a more systematic mathematical framework of nonlocal problems was developed in [11, 12] in parallel to the analysis for classic partial differential equations. Since the exact/analytic solutions of these nonlocal models are usually not available, numerical methods play an important role in studying these models. Bates, Brown, and Han [5] considered a finite difference discretization of the NAC equation with an integrable kernel and developed an L^∞ stable and convergent numerical scheme by treating the nonlinear and nonlocal terms explicitly. A similar technique was applied on the NAC-type problem coupled with a heat equation, and an L^∞ stable and convergent numerical scheme was obtained [2]. For nonlocal diffusion models with more general kernels and variable boundary conditions, finite difference and finite element approximations were addressed in [14, 40, 42, 50]. To illustrate the limit behaviors of the numerical solution of the nonlocal model to the exact solution of the corresponding local counterpart, Tian and Du

proposed in [43] the concept of *asymptotic compatibility*, and the spectral-Galerkin approximation of the NAC equation was then proved to be asymptotically compatible in [15]. The convergence of asymptotically compatible schemes is insensitive to the choices of modeling and discretization parameters so that such schemes provide robust numerical approximations of nonlocal models.

As a nonlocal analogue of the LAC equation (1.5), the NAC equation (1.1) possesses some similar properties. First, it can be shown that the NAC equation (1.1) satisfies a *maximum principle*: if the absolute values of initial and boundary data are bounded by 1, then the absolute value of the entire solution is also bounded by 1, i.e.,

$$\|u(\cdot, t)\|_{L^\infty} \le 1 \quad \forall\, t > 0.$$

Second, as a phase-field-type model, the NAC equation (1.1a) can be viewed as an L^2 gradient flow with respect to the energy functional

$$(1.6) \qquad E(u) = \int_\Omega \Big(\frac{1}{4}(u^2(\boldsymbol{x}) - 1)^2 - \frac{\varepsilon^2}{2} u(\boldsymbol{x}) \mathcal{L}_\delta u(\boldsymbol{x}) \Big)\, \mathrm{d}\boldsymbol{x},$$

and thus the solution u of (1.1) decreases the energy (1.6) in time, that is,

$$(1.7) \qquad E(u(t_2)) \le E(u(t_1)) \quad \forall\, t_2 \ge t_1 \ge 0,$$

which is often called the energy dissipation law. These two properties are important in the study of the stability of the solution of (1.1), and whether they could be inherited in the discrete level is a significant issue in numerical simulations. A major objective of this work is to develop maximum principle preserving and energy stable numerical schemes for approximating the NAC equation (1.1).

Energy stability has been widely investigated for numerical schemes of classic PDE-based phase field models, such as convex splitting schemes [34, 45], stabilized schemes [32, 33, 36, 46], invariant energy quadratization methods [47, 48], and so on. It is interesting to study whether similar analysis can be applied to nonlocal phase field models due to the lack of the high-order diffusion term. Guan, Wang, and Wise [22] constructed a convex splitting scheme for the nonlocal Cahn–Hilliard equation by treating the nonlinear term implicitly and setting the nonlocal term into the explicit part. Their scheme allows one to evaluate the nonlocal term explicitly only once each time step, but the nonlinear iterations are still inevitable. In order to avoid the nonlinear iterations, a linear stabilization strategy was adopted in [13] to develop stabilized linear schemes, which can be solved efficiently by using the fast Fourier transform. The energy stability of the fully discrete schemes were only shown under the assumption that the stabilizer depends implicitly on the uniform bound of the numerical solution.

The numerical method we will adopt in this work is the exponential time differencing (ETD) method, which involves exact integration of the governing equations followed by an explicit approximation of a temporal integral involving the nonlinear terms. The ETD scheme was systematically studied in [6] and then further developed by Cox and Matthews with applications on stiff systems [9], where higher-order multistep and Runge–Kutta versions of these schemes were described. Hochbruck and Ostermann provided several nice reviews of the ETD Runge–Kutta methods [24] and the ETD multistep methods [25]. In addition, the convergence of these methods were analyzed in detail under the analytical framework therein. The linear stabilities of some ETD and modified ETD schemes were investigated by Du and Zhu [17, 18].

A distinctive feature of ETD schemes is the exact evaluation of the contribution of the linear part, which provides satisfactory stability and accuracy even though the linear terms have strong stiffness. Such an advantage leads to some successful applications of ETD schemes on phase field models which usually yield highly stiff ODE systems after suitable spatial discretizations. Ju et al. developed stable and compact ETD schemes and their fast implementations for Allen–Cahn [29, 51], Cahn–Hilliard [28], and elastic bending energy models [44] by utilizing suitable linear splitting techniques. All the proposed ETD schemes are explicit and thus highly efficient for practical implementations. A localized compact ETD algorithm based on the overlapping domain decomposition was first used in [49] for extreme-scale phase field simulations of three-dimensional coarsening dynamics in the supercomputer, and the results showed excellent parallel scalability of the method. In [27], the ETD multistep method was applied on the epitaxial growth model without slope selection [31]. The energy stability and the error estimates were established rigorously, making it the first work to analyze the energy stability and convergence of the ETD schemes for phase field models in the theoretical level. To complete the theoretical analysis, there is no need for any assumptions on the numerical solutions due to the specific property of the logarithm term in the no-slope-selection model. However, for other phase field models, such as the Cahn–Hilliard equation, the assumptions on the uniform boundedness of the numerical solutions or the Lipschitz continuity of some nonlinear functions are inevitable to ensuring the energy stability. Therefore, for the models whose solutions satisfy the maximum principle essentially, it is highly desired to develop numerical approximations preserving the maximum principle in the discrete sense.

One of the typical phase field models satisfying the maximum principle is the LAC equation (1.5). Recently, there have been some investigations on the maximum principle preserving numerical schemes for (1.5). Tang and Yang [39] proved that the first order implicit-explicit schemes, with or without the stabilizing term, preserve the maximum principle under some condition on the time step size. Then the energy stability and the maximum-norm error estimates are obtained by using the discrete maximum principle. Shen, Tang, and Yang [35] generalized the results presented in [39] to the case of the Allen–Cahn-like equation in a more abstract form with the potential and mobility satisfying certain conditions. Hou, Tang, and Yang [26] studied the numerical approximation of the fractional Allen–Cahn equation by considering the conventional Crank–Nicolson scheme. They proved that the Crank–Nicolson scheme preserves the maximum principle, and this is the first work on the second order schemes preserving the maximum principle. More than ten years ago, Du and Zhu [18] showed that the first order ETD scheme in the space-continuous version for (1.5) satisfies the maximum principle, where some properties of the heat kernel were used in their proof. However, the fully discrete ETD schemes were never studied.

The organization of this paper is as follows. In section 2, we construct the first and second order ETD time-stepping schemes for the NAC equation with the quadrature-based finite difference approximation used for spatial discretization. Efficient implementation issues of the schemes are also briefly discussed. In section 3, both schemes are shown to satisfy the discrete maximum principle unconditionally. Error estimates and asymptotic compatibility of the schemes are obtained in section 4, and the discrete energy stability is proved in section 5. Various numerical experiments are carried out in section 6 to verify the theoretical results and to investigate the effects of the nonlocal parameters. Finally, some concluding remarks are given in section 7.

2. Fully discrete exponential time differencing schemes. In this section, we present the fully discrete ETD schemes for the NAC equation in general dimensions, where the finite difference method, based on the contribution made in [14], is adopted for the spatial discretization of the nonlocal diffusion operator. In particular, we also give the specific expression of the discrete nonlocal operator in 2D later.

2.1. Quadrature-based finite difference semidiscretization. Given a positive integer N, we set $h = X/N$ as the uniform square mesh size and define $\boldsymbol{x_i} = h\boldsymbol{i}$ as the nodes in the mesh, where $\boldsymbol{i} \in \mathbb{Z}^d$ denotes a multi-index. Let Ω_h be the set of nodes in $\overline{\Omega}$. At any node $\boldsymbol{x_i}$, the nonlocal operator (1.2) can be rewritten as

$$(2.1) \qquad \mathcal{L}_\delta u(\boldsymbol{x_i}) = \frac{1}{2} \int_{B_\delta(\boldsymbol{0})} \frac{u(\boldsymbol{x_i} + \boldsymbol{s}) + u(\boldsymbol{x_i} - \boldsymbol{s}) - 2u(\boldsymbol{x_i})}{|\boldsymbol{s}|^2} |\boldsymbol{s}|_1 \cdot \frac{|\boldsymbol{s}|^2}{|\boldsymbol{s}|_1} \rho_\delta(|\boldsymbol{s}|) \, \mathrm{d}\boldsymbol{s},$$

where $|\cdot|_1$ stands for the vector 1-norm. Then a quadrature-based finite difference discretization of the nonlocal operator (2.1) can be defined as [14]

$$\mathcal{L}_{\delta,h} u(\boldsymbol{x_i}) = \frac{1}{2} \int_{B_\delta(\boldsymbol{0})} \mathcal{I}_h \left(\frac{u(\boldsymbol{x_i} + \boldsymbol{s}) + u(\boldsymbol{x_i} - \boldsymbol{s}) - 2u(\boldsymbol{x_i})}{|\boldsymbol{s}|^2} |\boldsymbol{s}|_1 \right) \frac{|\boldsymbol{s}|^2}{|\boldsymbol{s}|_1} \rho_\delta(|\boldsymbol{s}|) \, \mathrm{d}\boldsymbol{s},$$

where $\mathcal{I}_h$ represents the piecewise d-multilinear interpolation operator with respect to $\boldsymbol{s}$ associated with the mesh. More precisely, for a function $v(\boldsymbol{s})$, the interpolation $\mathcal{I}_h v(\boldsymbol{s})$ is piecewise linear with respect to each component of the spatial variable $\boldsymbol{s}$ and

$$\mathcal{I}_h v(\boldsymbol{s}) = \sum_{\boldsymbol{s_j}} v(\boldsymbol{s_j}) \psi_{\boldsymbol{j}}(\boldsymbol{s}),$$

where $\psi_{\boldsymbol{j}}$ is the piecewise d-multilinear basis function satisfying $\psi_{\boldsymbol{j}}(\boldsymbol{s_i}) = 0$ when $\boldsymbol{i} \neq \boldsymbol{j}$ and $\psi_{\boldsymbol{j}}(\boldsymbol{s_j}) = 1$. Therefore, the resulting quadrature-based finite difference discretization of the nonlocal operator (2.1) reads
(2.2)

$$\mathcal{L}_{\delta,h} u(\boldsymbol{x_i}) = \sum_{\boldsymbol{0} \neq \boldsymbol{s_j} \in B_\delta(\boldsymbol{0})} \frac{u(\boldsymbol{x_i} + \boldsymbol{s_j}) + u(\boldsymbol{x_i} - \boldsymbol{s_j}) - 2u(\boldsymbol{x_i})}{|\boldsymbol{s_j}|^2} |\boldsymbol{s_j}|_1 \beta_\delta(\boldsymbol{s_j}), \quad \boldsymbol{x_i} \in \Omega_h,$$

where the periodicity conditions are used for the nodes not in Ω_h, and

$$\beta_\delta(\boldsymbol{s_j}) = \frac{1}{2} \int_{B_\delta(\boldsymbol{0})} \psi_{\boldsymbol{j}}(\boldsymbol{s}) \frac{|\boldsymbol{s}|^2}{|\boldsymbol{s}|_1} \rho_\delta(|\boldsymbol{s}|) \, \mathrm{d}\boldsymbol{s}.$$

It is easy to check that the operator $\mathcal{L}_{\delta,h}$ is self-adjoint and negative semidefinite.

The discretized scheme (2.2) is proposed in [14] for the problem with a homogeneous Dirichlet-type nonlocal constraint, and it has been proved [14, 41] that, for any fixed $\delta > 0$, the discrete operators $\mathcal{L}_{\delta,h}$ is consistent with $\mathcal{L}_\delta$ with the errors $\mathcal{O}(h^2)$ as $h \to 0$. For the case of periodic boundary condition considered here, all similar estimates also hold, so we give the following consistency estimates without proof.

LEMMA 2.1. *Assume that $u \in C_{\mathrm{per}}^4(\overline{\Omega})$; then it holds that*

$$(2.3) \qquad\qquad \max_{\boldsymbol{x_i} \in \Omega_h} |\mathcal{L}_{\delta,h} u(\boldsymbol{x_i}) - \mathcal{L}_\delta u(\boldsymbol{x_i})| \leq Ch^2 \|u\|_{C^4},$$

where $C > 0$ is a constant independent of δ and h.

By ordering the nodes in the lexicographical order, we can obtain the nonlocal stiffness matrix, denoted by $D_h \in \mathbb{R}^{dN \times dN}$, associated with $\mathcal{L}_{\delta,h}$. It is obvious that D_h is symmetric, negative semidefinite, and weakly diagonally dominant with all negative diagonal entries. The space-discrete scheme of (1.1) is to find a vector-valued function $U : [0,T] \to \mathbb{R}^{dN}$ such that

$$(2.4a) \qquad \frac{\mathrm{d}U}{\mathrm{d}t} = \varepsilon^2 D_h U + U - U^{.3}, \quad t \in (0,T],$$

$$(2.4b) \qquad U(0) = U_0,$$

where $U^{.3} = (U_1^3, U_2^3, \ldots, U_{dN}^3)^T$ and $U_0 \in \mathbb{R}^{dN}$ is given by the initial data. For the sake of the stability of the time-stepping schemes developed later, we introduce a *stabilizing parameter* $\kappa > 0$ and define

$$(2.5) \qquad L_h := -\varepsilon^2 D_h + \kappa I_{dN}, \qquad f(U) := (\kappa + 1)U - U^{.3},$$

where I_{dN} is the $dN \times dN$ identity matrix, so L_h is symmetric, positive definite, and strictly diagonally dominant with all positive diagonal entries. Then the ODE system (2.4a) could be written as

$$\frac{\mathrm{d}U}{\mathrm{d}t} + L_h U = f(U),$$

whose solution satisfies

$$(2.6) \qquad U(t+\tau) = \mathrm{e}^{-L_h \tau} U(t) + \int_0^\tau \mathrm{e}^{-L_h(\tau-s)} f(U(t+s))\, \mathrm{d}s \quad \forall t \geq 0,\ \tau > 0.$$

In the above, we have used a property of the differentiation of matrix exponentials (see Lemma 2.2 (5)). We list below some other properties of matrix functions useful to the analysis later.

LEMMA 2.2 (see [23]). *Let ϕ be defined on the spectrum of $A \in \mathbb{C}^{m \times m}$, that is, the values*

$$\phi^{(j)}(\lambda_i), \qquad 0 \leq j \leq n_i - 1,\ 1 \leq i \leq m,$$

exist, where $\{\lambda_i\}_{i=1}^m$ are the eigenvalues of A and n_i is the order of the largest Jordan block where λ_i appears. Then

(1) *$\phi(A)$ commutes with A;*
(2) *$\phi(A^T) = \phi(A)^T$;*
(3) *the eigenvalues of $\phi(A)$ are $\{\phi(\lambda_i) : 1 \leq i \leq m\}$;*
(4) *$\phi(P^{-1}AP) = P^{-1}\phi(A)P$ for any nonsingular matrix $P \in \mathbb{C}^{m \times m}$;*
(5) *$\frac{\mathrm{d}}{\mathrm{d}s}(\mathrm{e}^{As}) = A\mathrm{e}^{As} = \mathrm{e}^{As}A$ for any $s \in \mathbb{R}$.*

2.2. Exponential time differencing schemes for time-stepping. Given a positive integer K_t, we divide the time interval by $\{t_n = n\tau : 0 \leq n \leq K_t\}$ with a uniform time step $\tau = T/K_t$. Setting $t = t_n$ in (2.6) gives us

$$U(t_{n+1}) = \mathrm{e}^{-L_h \tau} U(t_n) + \int_0^\tau \mathrm{e}^{-L_h(\tau-s)} f(U(t_n + s))\, \mathrm{d}s.$$

The first order ETD (ETD1) scheme comes from approximating $f(U(t_n + s))$ by $f(U(t_n))$ in $s \in [0,\tau]$ and calculating the resulting integral exactly [9]. The ETD1 scheme of (1.1) is as follows: for $n = 0, 1, \ldots, K_t - 1$,

$$(2.7) \qquad U^{n+1} = \mathrm{e}^{-L_h \tau} U^n + \int_0^\tau \mathrm{e}^{-L_h(\tau-s)} f(U^n)\, \mathrm{d}s,$$

that is,

$$(2.8) \qquad U^{n+1} = \phi_0(L_h\tau)U^n + \tau\phi_1(L_h\tau)f(U^n),$$

where

$$\phi_0(a) := \mathrm{e}^{-a}, \quad \phi_1(a) := \frac{1-\mathrm{e}^{-a}}{a}, \quad a \neq 0.$$

The second order ETD Runge–Kutta (ETDRK2) scheme is obtained by approximating $f(U(t_n+s))$ by a linear interpolation based on $f(U(t_n))$ and $f(\widetilde{U}^{n+1})$, where $\widetilde{U}^{n+1}$ is an approximation of $U(t_{n+1})$. The ETDRK2 scheme of (1.1) takes the following form: for $n = 0, 1, \ldots, K_t - 1$,

$$(2.9a) \qquad \widetilde{U}^{n+1} = \mathrm{e}^{-L_h\tau}U^n + \int_0^\tau \mathrm{e}^{-L_h(\tau-s)}f(U^n)\,\mathrm{d}s,$$

$$(2.9b) \qquad U^{n+1} = \mathrm{e}^{-L_h\tau}U^n + \int_0^\tau \mathrm{e}^{-L_h(\tau-s)}\left[\left(1-\frac{s}{\tau}\right)f(U^n) + \frac{s}{\tau}f(\widetilde{U}^{n+1})\right]\mathrm{d}s,$$

or, equivalently,

$$(2.10a) \qquad \widetilde{U}^{n+1} = \phi_0(L_h\tau)U^n + \tau\phi_1(L_h\tau)f(U^n),$$

$$(2.10b) \qquad U^{n+1} = \widetilde{U}^{n+1} + \tau\phi_2(L_h\tau)(f(\widetilde{U}^{n+1}) - f(U^n)),$$

where

$$\phi_2(a) := \frac{\mathrm{e}^{-a}-1+a}{a^2}, \quad a \neq 0.$$

We know that $\phi_0(a)$, $\phi_1(a)$, and $\phi_2(a)$ are all positive when $a > 0$.

2.3. Efficient implementations of the ETD schemes. We close this section by giving a brief illustration of the practical implementation of the proposed schemes (2.8) and (2.10). Using the 2D case as the example, we first give the explicit formula of the discrete operator $\mathcal{L}_{\delta,h}$ (as illustrated in [14]) and then discuss efficient implementation of the actions of the matrix exponentials.

Let $u_{i,j}$ be the nodal value of the numerical solution at the mesh point $(x_i, y_j) \in \Omega_h \subset \mathbb{R}^2$, and let $r = [\delta/h] + 1$ be the smallest integer larger than δ/h. Then we have

$$\mathcal{L}_{\delta,h}u_{i,j} = \sum_{p=0}^{r}\sum_{q=0}^{r} c_{p,q}(u_{i+p,j+q} + u_{i-p,j+q} + u_{i+p,j-q} + u_{i-p,j-q} - 4u_{i,j}),$$

where $c_{0,0} = 0$ and

$$(2.11) \qquad c_{p,q} = \frac{p+q}{(p^2+q^2)h}\iint_{B_\delta^+}\psi_{p,q}(x,y)\rho_\delta(\sqrt{x^2+y^2})\frac{x^2+y^2}{x+y}\,\mathrm{d}x\mathrm{d}y,$$

with $\psi_{p,q}$ denoting the bilinear basis function located at the point (ph, qh) and B_δ^+ the first quadrant of the disc centered at the origin with radius δ. Note that $c_{p,q} = c_{q,p}$ for any p and q. One can apply efficient quadrature rules on the double integrals in (2.11).

We represent $U^n \in \mathbb{R}^{N \times N}$ in the matrix form with entries $u_{i,j}^n$ and define the operator $\mathcal{L}_h = \kappa\mathcal{I} - \varepsilon^2\mathcal{L}_{\delta,h}$ whose matrix form is given by L_h defined in (2.5), where $\mathcal{I}$ is the identity mapping. The key process of calculating U^{n+1} from the scheme (2.8) or (2.10) is the efficient implementation of the actions of the operator exponentials

$\phi_\gamma(\mathcal{L}_h\tau)$, $\gamma = 0, 1, 2$. Since $\mathcal{L}_h$ comes from the discretization of $\mathcal{L}_\delta$ with the periodic boundary condition, the exponentials $\phi_\gamma(\mathcal{L}_h\tau)$ can be implemented by the 2D discrete Fourier transform (DFT). More precisely, if we denote by $\mathcal{F}$ the 2D DFT operator, then, for any $V = (V_{k,l}) \in \mathbb{C}^{N \times N}$, the action of the operator $\widehat{\mathcal{L}}_h := \mathcal{F}\mathcal{L}_h\mathcal{F}^{-1}$ can be implemented via

$$(\widehat{\mathcal{L}}_h V)_{k,l} = \lambda_{k,l} V_{k,l}, \quad 1 \leq k, l \leq N,$$

where $\lambda_{k,l}$'s, the eigenvalues of $\mathcal{L}_h$, are given by

$$\lambda_{k,l} = \kappa + 4\varepsilon^2 \sum_{p=0}^{r} \sum_{q=0}^{r} c_{p,q}\left(1 - \cos\frac{2\pi(k-1)p}{N}\cos\frac{2\pi(l-1)q}{N}\right), \quad 1 \leq k, l \leq N.$$

According to Lemma 2.2 (4), we have

$$\phi_\gamma(\mathcal{L}_h\tau) = \mathcal{F}^{-1}\phi_\gamma(\widehat{\mathcal{L}}_h\tau)\mathcal{F}, \quad (\phi_\gamma(\widehat{\mathcal{L}}_h\tau)V)_{k,l} = \phi_\gamma(\lambda_{k,l}\tau)V_{k,l}, \quad \gamma = 0, 1, 2.$$

The actions of $\mathcal{F}$ and $\mathcal{F}^{-1}$ can be implemented by the 2D fast Fourier transform (FFT) and its inverse transform, respectively. Such implementation can be naturally generalized to higher-dimensional spaces, and the computational complexity is thus $\mathcal{O}(N^d \log N)$ per time step.

3. Discrete maximum principle. Denote by $\|\cdot\|_\infty$ the standard vector or matrix ∞-norm and by $\|\cdot\|_2$ the standard vector or matrix 2-norm. The following lemma is a special case of Theorem 2 in [30].

LEMMA 3.1. *Let $A = (a_{ij}) \in \mathbb{R}^{m \times m}$ with $a_{ii} < 0$, $1 \leq i \leq m$, and there exists $\kappa > 0$ such that*

$$|a_{ii}| \geq \sum_{\substack{j=1 \\ j \neq i}}^{m} |a_{ij}| + \kappa, \quad 1 \leq i \leq m.$$

Then the nontrivial solution $\theta = \theta(t)$ of the linear differential system

$$(3.1) \qquad \frac{\mathrm{d}\theta}{\mathrm{d}t} = A\theta, \quad t > 0,$$

satisfies

$$\|\theta(t_2)\|_\infty \leq \mathrm{e}^{-\kappa(t_2-t_1)}\|\theta(t_1)\|_\infty \quad \forall t_2 \geq t_1 \geq 0.$$

The following result is a key ingredient in proving the discrete maximum principle.

LEMMA 3.2. *For any $\kappa > 0$ and $\tau > 0$, we always have $\|\mathrm{e}^{-L_h\tau}\|_\infty \leq \mathrm{e}^{-\kappa\tau}$.*

Proof. Since L_h is strictly diagonally dominant with all positive diagonal entries, the matrix $A := -L_h$ satisfies the conditions of Lemma 3.1 with $\kappa > 0$. For any nonzero $\theta_0 \in \mathbb{R}^{dN}$, we know that the solution of the linear differential system (3.1) with the initial value $\theta(0) = \theta_0$ is given by $\theta(t) = \mathrm{e}^{-L_h t}\theta_0$ and, by using Lemma 3.1, satisfies

$$\|\mathrm{e}^{-L_h\tau}\theta_0\|_\infty = \|\theta(\tau)\|_\infty \leq \mathrm{e}^{-\kappa\tau}\|\theta_0\|_\infty, \quad \tau > 0.$$

Therefore, the result follows from the arbitrariness of θ_0. $\square$

Remark 3.1. Although our deduction above is restricted to the periodic boundary condition case, the result of Lemma 3.2 is also suitable for the case of the Dirichlet boundary condition, since the corresponding nonlocal stiffness matrix D_h is still weakly diagonally dominant with all negative diagonal entries. The analysis results in this paper could be obtained similarly for the Dirichlet boundary condition.

Since the nonlinear mapping $f : \mathbb{R}^{dN} \to \mathbb{R}^{dN}$ defined in (2.5) is actually a set of dN independent one-variable functions, we just need to consider any one of them.

LEMMA 3.3. *Define* $f_0(\xi) := (\kappa + 1)\xi - \xi^3$ *for any* $\xi \in \mathbb{R}$. *If* $\kappa \geq 2$, *then*

$$|f_0(\xi)| \leq \kappa \quad \forall \, \xi \in [-1, 1].$$

Proof. Obviously, $f_0(-1) = -\kappa$ and $f_0(1) = \kappa$. For any $\xi \in [-1, 1]$, if $\kappa \geq 2$, we have

$$(3.2) \qquad f_0'(\xi) = \kappa + 1 - 3\xi^2 \geq \kappa - 2 \geq 0,$$

which gives us the result.   □

THEOREM 3.4. *Assume that the initial data satisfies* $\|u_0\|_{L^\infty} \leq 1$. *For any time step size* $\tau > 0$, *ETD1 scheme* (2.7) *preserves the discrete maximum principle, i.e.,*

$$\|U^n\|_\infty \leq 1 \quad \forall \, n \geq 0,$$

provided the stabilizing parameter $\kappa \geq 2$.

Proof. We prove this theorem by induction. Obviously, $\|U^0\|_\infty \leq \|u_0\|_{L^\infty} \leq 1$. Now assume that the result holds for $n = k$, i.e., $\|U^k\|_\infty \leq 1$. Next we check whether this holds for $n = k + 1$. According to the scheme (2.7), we have

$$\|U^{k+1}\|_\infty \leq \|\mathrm{e}^{-L_h \tau}\|_\infty \|U^k\|_\infty + \int_0^\tau \|\mathrm{e}^{-L_h(\tau - s)}\|_\infty \, \mathrm{d}s \cdot \|f(U^k)\|_\infty.$$

It follows from Lemma 3.2 that

$$(3.3) \quad \|\mathrm{e}^{-L_h \tau}\|_\infty \leq \mathrm{e}^{-\kappa \tau}, \qquad \int_0^\tau \|\mathrm{e}^{-L_h(\tau - s)}\|_\infty \, \mathrm{d}s \leq \int_0^\tau \mathrm{e}^{-\kappa(\tau - s)} \, \mathrm{d}s = \frac{1 - \mathrm{e}^{-\kappa \tau}}{\kappa}.$$

Using Lemma 3.3 and $\|U^k\|_\infty \leq 1$, we have $\|f(U^k)\|_\infty \leq \kappa$. Consequently,

$$\|U^{k+1}\|_\infty \leq \mathrm{e}^{-\kappa \tau} \cdot 1 + \frac{1 - \mathrm{e}^{-\kappa \tau}}{\kappa} \cdot \kappa = 1,$$

which completes the proof.   □

THEOREM 3.5. *Assume that the initial data satisfies* $\|u_0\|_{L^\infty} \leq 1$. *For any time step size* $\tau > 0$, *ETDRK2 scheme* (2.9) *preserves the discrete maximum principle, i.e.,*

$$\|U^n\|_\infty \leq 1 \quad \forall \, n \geq 0,$$

provided the stabilizing parameter $\kappa \geq 2$.

Proof. We again prove this by induction. Obviously, it holds that $\|U^0\|_\infty \leq \|u_0\|_{L^\infty} \leq 1$. Now assume that the result holds for $n = k$, i.e., $\|U^k\|_\infty \leq 1$. Next we check this for $n = k + 1$. According to formula (2.9a) and the proof of Theorem 3.4, we have $\|\widetilde{U}^{k+1}\|_\infty \leq 1$. According to formula (2.9b), we have
$$(3.4)$$
$$\|U^{k+1}\|_\infty \leq \|\mathrm{e}^{-L_h \tau}\|_\infty \|U^k\|_\infty + \int_0^\tau \|\mathrm{e}^{-L_h(\tau - s)}\|_\infty \left\| \left(1 - \frac{s}{\tau}\right) f(U^k) + \frac{s}{\tau} f(\widetilde{U}^{k+1}) \right\|_\infty \, \mathrm{d}s.$$

Since $\|U^k\|_\infty \leq 1$ and $\|\widetilde{U}^{k+1}\|_\infty \leq 1$, using Lemma 3.3, we have

$$\|f(U^k)\|_\infty \leq \kappa, \quad \|f(\widetilde{U}^{k+1})\|_\infty \leq \kappa,$$

and then, for $s \in (0, \tau)$,

$$\left\| \left(1 - \frac{s}{\tau}\right) f(U^k) + \frac{s}{\tau} f(\widetilde{U}^{k+1}) \right\|_\infty \leq \left(1 - \frac{s}{\tau}\right) \kappa + \frac{s}{\tau} \kappa = \kappa.$$

Again, by using (3.3), we obtain from (3.4) that

$$\|U^{k+1}\|_\infty \leq e^{-\kappa\tau} \cdot 1 + \frac{1 - e^{-S\tau}}{\kappa} \cdot \kappa = 1,$$

which completes the proof. $\qquad\square$

Remark 3.2. We will then always require $\kappa \geq 2$ for the proposed ETD1 and ETDRK2 schemes in the rest of the paper so that they preserve the discrete maximum principle.

4. Error estimates and asymptotic compatibility. We will analyze two types of convergence behaviors of the numerical solution of ETD1 scheme (2.7) and ETDRK2 scheme (2.9), respectively. First, for any fixed $\delta > 0$, we prove that the numerical solution converges to the exact solution of NAC equation (1.1) as the spatial mesh size h and the time step size τ go to zero. Second, we show that the numerical solution converges to the exact solution of LAC equation (1.5) as the horizon parameter δ, the spatial size h, and the temporal step τ approach zero. The latter convergence behavior of the numerical solution is often called the *asymptotic compatibility* [43] in nonlocal modeling.

We first establish the L^∞ error estimates for the numerical solution produced by ETD1 scheme (2.7) for NAC equation (1.1) with any fixed $\delta > 0$. Denote by I^h the operator limiting a function on the mesh Ω_h.

THEOREM 4.1. *Given a fixed $\delta > 0$, assume that the exact solution u of the NAC equation* (1.1) *belongs to $C^1([0,T]; C^4_{\mathrm{per}}(\overline{\Omega}))$ and $\{U^n\}_{n=0}^{K_t}$ is generated by the ETD1 scheme* (2.7) *with $U^0 = I^h u_0$. If $\|u_0\|_{L^\infty} \leq 1$, then we have*

$$(4.1) \qquad \|U^n - I^h u(t_n)\|_\infty \leq C e^{t_n}(h^2 + \tau), \quad t_n \leq T,$$

for any $h > 0$ and $\tau > 0$, where the constant $C > 0$ depends on the $C^1([0,T]; C^4_{\mathrm{per}}(\overline{\Omega}))$-norm of u, but independent of δ, h, and τ.

Proof. Recalling the construction of ETD1 scheme (2.7), we observe that, for a known U^n, the solution U^{n+1} is actually given by $U^{n+1} = W_1(\tau)$ with the function $W_1 : [0, \tau] \to \mathbb{R}^{dN}$ determined by the following evolution equation:

$$(4.2) \qquad \begin{cases} \dfrac{\mathrm{d}W_1(s)}{\mathrm{d}s} = -\kappa W_1(s) + \varepsilon^2 D_h W_1(s) + f(U^n), & s \in (0, \tau), \\ W_1(0) = U^n. \end{cases}$$

Then, for NAC equation (1.1), we can give a similar illustration as follows: For given $u(\boldsymbol{x}, t_n)$, the solution $u(\boldsymbol{x}, t_{n+1})$ is determined by $u(\boldsymbol{x}, t_{n+1}) = w(\boldsymbol{x}, \tau)$ with the function $w(\boldsymbol{x}, s)$ satisfying

$$(4.3) \qquad \begin{cases} \dfrac{\partial w}{\partial s} = -\kappa w + \varepsilon^2 \mathcal{L}_\delta w + f_0(w), & \boldsymbol{x} \in \Omega, \ s \in (0, \tau), \\ w(\cdot, s) \text{ is } \Omega\text{-periodic}, & s \in [0, \tau], \\ w(\boldsymbol{x}, 0) = u(\boldsymbol{x}, t_n), & \boldsymbol{x} \in \overline{\Omega}. \end{cases}$$

Let $e_1(s) = W_1(s) - I^h w(s)$. Then the difference between (4.2) and (4.3) yields

(4.4)
$$\begin{cases} \dfrac{de_1(s)}{ds} = -L_h e_1(s) + f(U^n) - f(I^h u(t_n)) + R_{h\tau}^{(1)}(s), & s \in (0, \tau), \\ e_1(0) = U^n - I^h u(t_n) =: e_1^n, \end{cases}$$

where $R_{h\tau}^{(1)}(s)$ is the truncated error, that is,

$$R_{h\tau}^{(1)}(s) = \varepsilon^2 (D_h I^h u(t_n + s) - I^h \mathcal{L}_\delta u(t_n + s)) + f(I^h u(t_n)) - f(I^h u(t_n + s)).$$

Since $|f'(\xi)| \le \kappa + 1$ for any $\xi \in [-1, 1]$ and both the exact and numerical solutions satisfy the maximum principles, we have

(4.5) $\qquad \|f(U^n) - f(I^h u(t_n))\|_\infty \le (\kappa + 1)\|U^n - I^h u(t_n)\|_\infty = (\kappa + 1)\|e_1^n\|_\infty.$

According to the consistency result given by Lemma 2.1, if the exact solution u is sufficiently smooth, at least $u \in C^1([0, T]; C_{\text{per}}^4(\overline{\Omega}))$, then we have

(4.6) $\qquad \|D_h I^h u(t) - I^h \mathcal{L}_\delta u(t)\|_\infty \le C_1 h^2 \quad \forall\, t \in [0, T],$

and for $s \in (0, \tau)$,

$$\|f(I^h u(t_n)) - f(I^h u(t_n + s))\|_\infty \le (\kappa + 1)\|I^h(u(t_n) - u(t_n + s))\|_\infty \le C_2(\kappa + 1)\tau,$$

where C_1 and C_2 depend on the $C^1([0, T]; C_{\text{per}}^4(\overline{\Omega}))$-norm of u, but independent of δ, h, and τ. Thus, we obtain

$$\|R_{h\tau}^{(1)}(s)\|_\infty \le C(h^2 + \tau) \quad \forall\, s \in (0, \tau),$$

where $C = \max\{C_1 \varepsilon^2, C_2(\kappa + 1)\}$. Integrating the ODE in (4.4) leads to

$$e_1(t) = e^{-L_h t} e_1(0) + \int_0^t e^{-L_h(t-s)}[f(U^n) - f(I^h u(t_n)) + R_{h\tau}^{(1)}(s)]\, ds, \quad t \in [0, \tau].$$

Setting $t = \tau$ and using (3.3), we have

$$\|e_1^{n+1}\|_\infty \le \|e^{-L_h \tau}\|_\infty \|e_1^n\|_\infty + [(\kappa + 1)\|e_1^n\|_\infty + C(h^2 + \tau)] \int_0^\tau \|e^{-L_h(\tau - s)}\|_\infty\, ds$$

$$\le e^{-\kappa\tau}\|e_1^n\|_\infty + \frac{1 - e^{-\kappa\tau}}{\kappa}[(\kappa + 1)\|e_1^n\|_\infty + C(h^2 + \tau)]$$

$$= \left(1 + \frac{1 - e^{-\kappa\tau}}{\kappa}\right)\|e_1^n\|_\infty + \frac{1 - e^{-\kappa\tau}}{\kappa} C(h^2 + \tau)$$

(4.7) $\qquad \le (1 + \tau)\|e_1^n\|_\infty + C\tau(h^2 + \tau),$

where in the last step we have used the fact that $1 - e^{-s} \le s$ for any $s > 0$. By induction, we obtain

$$\|e_1^n\|_\infty \le (1 + \tau)^n \|e_1^0\|_\infty + C\tau(h^2 + \tau) \sum_{k=0}^{n-1} (1 + \tau)^k$$

$$= (1 + \tau)^n \|e_1^0\|_\infty + C[(1 + \tau)^n - 1](h^2 + \tau)$$

$$\le e^{n\tau}\|e_1^0\|_\infty + C e^{n\tau}(h^2 + \tau).$$

Therefore, we obtain (4.1) since $e_1^0 = 0$ and $n\tau = t_n$. $\qquad\qquad\square$

Now, we turn to the L^∞ error estimates for ETDRK2 scheme (2.9) with any fixed $\delta > 0$.

THEOREM 4.2. *Given a fixed $\delta > 0$, assume that the exact solution u of NAC equation* (1.1) *belongs to $C^2([0,T]; C^4_{\mathrm{per}}(\overline{\Omega}))$ and $\{U^n\}_{n=0}^{K_t}$ is generated by ETDRK2 scheme* (2.9) *with $U^0 = I^h u_0$. If $\|u_0\|_{L^\infty} \leq 1$, then we have*

$$(4.8) \qquad \|U^n - I^h u(t_n)\|_\infty \leq C e^{t_n} (h^2 + \tau^2), \quad t_n \leq T,$$

for any $h > 0$ and $0 < \tau \leq 1$, where the constant $C > 0$ depends on the $C^2([0,T]; C^4_{\mathrm{per}}(\overline{\Omega}))$-norm of u, but independent of δ, h, and τ.

Proof. For a known U^n, the solution U^{n+1} of ETDRK2 scheme (2.9) is actually given by $U^{n+1} = W_2(\tau)$, with the function $W_2 : [0,\tau] \to \mathbb{R}^{dN}$ determined by the evolution equation
(4.9)
$$\begin{cases} \dfrac{\mathrm{d}W_2(s)}{\mathrm{d}s} = -\kappa W_2(s) + \varepsilon^2 D_h W_2(s) + \left(1 - \dfrac{s}{\tau}\right) f(U^n) + \dfrac{s}{\tau} f(\widetilde{U}^{n+1}), \quad s \in (0,\tau), \\ W_2(0) = U^n, \end{cases}$$

where $\widetilde{U}^{n+1}$, defined by (2.9a), is given by $\widetilde{U}^{n+1} = W_1(\tau)$, with $W_1(s)$ satisfying (4.2). Let $e_2(s) = W_2(s) - I^h w(s)$. The difference between (4.9) and (4.3) leads to

$$(4.10) \qquad \begin{cases} \dfrac{\mathrm{d}e_2(s)}{\mathrm{d}s} = -L_h e_2(s) + \left(1 - \dfrac{s}{\tau}\right)[f(U^n) - f(I^h u(t_n))] \\ \qquad\qquad + \dfrac{s}{\tau}[f(\widetilde{U}^{n+1}) - f(I^h u(t_{n+1}))] + R^{(2)}_{h\tau}(s), \quad s \in (0,\tau), \\ e_2(0) = U^n - I^h u(t_n) =: e_2^n, \end{cases}$$

where $R^{(2)}_{h\tau}(s)$ is the truncated error given by

$$\begin{aligned} R^{(2)}_{h\tau}(s) = {}& \varepsilon^2 (D_h I^h u(t_n + s) - I^h \mathcal{L}_\delta u(t_n + s)) \\ & + \left[\left(1 - \frac{s}{\tau}\right) f(I^h u(t_n)) + \frac{s}{\tau} f(I^h u(t_{n+1})) - f(I^h u(t_n + s))\right]. \end{aligned}$$

According to error estimates for the linear interpolation, we have, for $s \in (0,\tau)$, that

$$\left\|\left(1 - \frac{s}{\tau}\right) f(I^h u(t_n)) + \frac{s}{\tau} f(I^h u(t_{n+1})) - f(I^h u(t_n + s))\right\| \leq C_3 \tau^2,$$

where C_3 depends on the $C^2([0,T]; C^4_{\mathrm{per}}(\overline{\Omega}))$-norm of u, but independent of δ, h, and τ. Thus, combined with (4.6), we obtain

$$\|R^{(2)}_{h\tau}(s)\|_\infty \leq C_4(h^2 + \tau^2) \quad \forall\, s \in (0,\tau),$$

where $C_4 = \max\{C_1 \varepsilon^2, C_3\}$. According to (4.7) in the proof for the ETD1 scheme, we have

$$\|\widetilde{U}^{n+1} - I^h u(t_{n+1})\|_\infty \leq (1 + \tau)\|U^n - I^h u(t_n)\|_\infty + C_5 \tau(h^2 + \tau),$$

where C_5 depends on the $C^1([0,T]; C^4_{\mathrm{per}}(\overline{\Omega}))$-norm of u. Then, using the Lipschitz continuity of f, we obtain

$$\begin{aligned} \|f(\widetilde{U}^{n+1}) - f(I^h u(t_{n+1}))\|_\infty &\leq (\kappa + 1)\|\widetilde{U}^{n+1} - I^h u(t_{n+1})\|_\infty \\ &\leq (\kappa + 1)(1 + \tau)\|e_2^n\|_\infty + C_5 \tau(\kappa + 1)(h^2 + \tau). \end{aligned}$$

Combining with (4.5), we have, for any $s \in (0, \tau)$, that

$$
\left\| \left(1 - \frac{s}{\tau}\right)[f(U^n) - f(I^h u(t_n))] + \frac{s}{\tau}[f(\widetilde{U}^{n+1}) - f(I^h u(t_{n+1}))] \right\|_\infty
$$
$$
\leq \left(1 - \frac{s}{\tau}\right)(\kappa + 1)\|e_2^n\|_\infty + \frac{s}{\tau}(\kappa + 1)(1 + \tau)\|e_2^n\|_\infty + C_5 s(\kappa + 1)(h^2 + \tau)
$$
$$
= (s + 1)(\kappa + 1)\|e_2^n\|_\infty + C_5 s(\kappa + 1)(h^2 + \tau).
$$

Integrating the ODE in (4.10) leads to

$$
e_2(t) = \mathrm{e}^{-L_h t} e_2(0) + \int_0^t \mathrm{e}^{-L_h(t-s)} \Big\{ \left(1 - \frac{s}{\tau}\right)[f(U^n) - f(I^h u(t_n))]
$$
$$
+ \frac{s}{\tau}[f(\widetilde{U}^{n+1}) - f(I^h u(t_{n+1}))] + R_{h\tau}^{(2)}(s) \Big\}\, \mathrm{d}s, \qquad t \in [0, \tau].
$$

Setting $t = \tau$ and using (3.3), we have

$$
\|e_2^{n+1}\|_\infty \leq \|\mathrm{e}^{-L_h \tau}\|_\infty \|e_2^n\|_\infty + [(\kappa + 1)\|e_2^n\|_\infty + C_4(h^2 + \tau^2)] \int_0^\tau \|\mathrm{e}^{-L_h(\tau-s)}\|_\infty\, \mathrm{d}s
$$
$$
+ [(\kappa + 1)\|e_2^n\|_\infty + C_5(\kappa + 1)(h^2 + \tau)] \int_0^\tau s \|\mathrm{e}^{-L_h(\tau-s)}\|_\infty\, \mathrm{d}s
$$
$$
\leq \mathrm{e}^{-\kappa\tau}\|e_2^n\|_\infty + \frac{1 - \mathrm{e}^{-\kappa\tau}}{\kappa}[(\kappa + 1)\|e_2^n\|_\infty + C_4(h^2 + \tau^2)]
$$
$$
+ \frac{\mathrm{e}^{-\kappa\tau} - 1 + \kappa\tau}{\kappa^2}[(\kappa + 1)\|e_2^n\|_\infty + C_5(\kappa + 1)(h^2 + \tau)]
$$
$$
= \left(1 + \tau + \frac{\mathrm{e}^{-\kappa\tau} - 1 + \kappa\tau}{\kappa^2}\right)\|e_2^n\|_\infty
$$
$$
+ \frac{1 - \mathrm{e}^{-\kappa\tau}}{\kappa}C_4(h^2 + \tau^2) + \frac{\mathrm{e}^{-\kappa\tau} - 1 + \kappa\tau}{\kappa^2}C_5(\kappa + 1)(h^2 + \tau)
$$
$$
\leq \left(1 + \tau + \frac{\tau^2}{2}\right)\|e_2^n\|_\infty + C_4\tau(h^2 + \tau^2) + \frac{1}{2}C_5(\kappa + 1)\tau(\tau h^2 + \tau^2)
$$
$$
\leq \left(1 + \tau + \frac{\tau^2}{2}\right)\|e_2^n\|_\infty + C\tau(h^2 + \tau^2),
$$

where $C = C_4 + \frac{1}{2}C_5(\kappa + 1)$. The condition $\tau \leq 1$ is used in the last step of the above derivation. By induction, we obtain

$$
\|e_2^n\|_\infty \leq \left(1 + \tau + \frac{\tau^2}{2}\right)^n \|e_2^0\|_\infty + C\tau(h^2 + \tau^2) \sum_{k=0}^{n-1} \left(1 + \tau + \frac{\tau^2}{2}\right)^k
$$
$$
\leq \left(1 + \tau + \frac{\tau^2}{2}\right)^n \|e_2^0\|_\infty + C\left[\left(1 + \tau + \frac{\tau^2}{2}\right)^n - 1\right](h^2 + \tau^2)
$$
$$
\leq \mathrm{e}^{n\tau}\|e_2^0\|_\infty + C\mathrm{e}^{n\tau}(h^2 + \tau^2),
$$

which then gives us (4.8).   □

Now, let us investigate the asymptotic compatibility of both the ETD1 and ET-DRK2 schemes. Combining (1.4) with the uniform estimates (2.3) of the consistency of $\mathcal{L}_{\delta,h}$, we obtain

$$
(4.11) \qquad \max_{\boldsymbol{x_i} \in \Omega_h} |\mathcal{L}_{\delta,h} u(\boldsymbol{x_i}) - \mathcal{L}_0 u(\boldsymbol{x_i})| \leq C(\delta^2 + h^2)\|u\|_{C^4},
$$

where $C > 0$ is a constant independent of δ and h. Denote by $\varphi(\boldsymbol{x}, t)$ the solution of the LAC equation (1.5). For given $\varphi(\boldsymbol{x}, t_n)$, the solution $\varphi(\boldsymbol{x}, t_{n+1})$ is determined by $\varphi(\boldsymbol{x}, t_{n+1}) = v(\boldsymbol{x}, \tau)$, with the function $v(\boldsymbol{x}, t)$ satisfying

(4.12)
$$\begin{cases} \dfrac{\partial v}{\partial t} = -\kappa v + \varepsilon^2 \mathcal{L}_0 v + f(v), & \boldsymbol{x} \in \Omega, \ t \in (0, \tau), \\ v(\cdot, t) \text{ is } \Omega\text{-periodic}, & t \in [0, \tau], \\ v(\boldsymbol{x}, 0) = \varphi(\boldsymbol{x}, t_n), & \boldsymbol{x} \in \overline{\Omega}. \end{cases}$$

Let $\widehat{e}(t) = W_1(t) - I^h v(t)$, where $W_1(t)$ is defined by (4.2). Then the difference between (4.2) and (4.12) yields

$$\begin{cases} \dfrac{\mathrm{d}\widehat{e}(t)}{\mathrm{d}t} = -L_h \widehat{e}(t) + f(U^n) - f(I^h \varphi(t_n)) + \widehat{R}_{h\tau}^\delta(t), & t \in (0, \tau), \\ \widehat{e}(0) = U^n - I^h \varphi(t_n) =: \widehat{e}^n, \end{cases}$$

where the remainder $\widehat{R}_{h\tau}^\delta(t)$ is given by

$$\widehat{R}_{h\tau}^\delta(t) = \varepsilon^2 (D_h I^h \varphi(t_n + t) - I^h \mathcal{L}_0 \varphi(t_n + t)) + f(I^h \varphi(t_n)) - f(I^h \varphi(t_n + t)),$$

and, according to the estimates (4.11) and the Lipschitz continuity of f under the condition $\kappa \geq 2$, is bounded by

$$\|\widehat{R}_{h\tau}^\delta(t)\|_\infty \leq C(\delta^2 + h^2 + \tau) \quad \forall t \in (0, \tau),$$

where $C > 0$ depends on ε, κ, and the $C^1([0, T]; C_{\mathrm{per}}^4(\overline{\Omega}))$-norm of φ, but independent of δ, h, and τ. By conducting analysis similar to what was done for error estimates, we can obtain the asymptotic compatibility of the numerical solution of ETD1 scheme (2.7). Such is also the case for ETDRK2 scheme (2.9). Therefore, we have the following results.

THEOREM 4.3 (asymptotic compatibility). *Assume that the solution φ of LAC equation (1.5) belongs to $C^1([0, T]; C_{\mathrm{per}}^4(\overline{\Omega}))$ (resp., $C^2([0, T]; C_{\mathrm{per}}^4(\overline{\Omega}))$) and $\{U^n\}_{n=0}^{K_t}$ is generated by ETD1 scheme (2.7) (resp., ETDRK2 scheme (2.9)) with $U^0 = I^h \varphi_0$. If $\|\varphi_0\|_{L^\infty} \leq 1$, then we have*

$$\|U^n - I^h \varphi(t_n)\|_\infty \leq C e^{t_n} (\delta^2 + h^2 + \tau), \quad t_n \leq T$$

$$(\text{resp.,} \ \|U^n - I^h \varphi(t_n)\|_\infty \leq C e^{t_n} (\delta^2 + h^2 + \tau^2), \quad t_n \leq T),$$

for any $\delta > 0$, $h > 0$, and $\tau > 0$ (resp., $\tau \in (0, 1]$), where the constant C depends on the $C^1([0, T]; C_{\mathrm{per}}^4(\overline{\Omega}))$-norm (resp., $C^2([0, T]; C_{\mathrm{per}}^4(\overline{\Omega}))$-norm) of φ, but independent of δ, h, and τ.

5. Discrete energy stability. We first show that ETD1 scheme (2.7) inherits the energy decay law (1.7) in the discrete sense, with respect to the discretized energy E_h defined by

$$E_h(U) = \frac{1}{4} \sum_{i=1}^{dN} (U_i^2 - 1)^2 - \frac{\varepsilon^2}{2} U^T D_h U \quad \forall U \in \mathbb{R}^{dN}.$$

THEOREM 5.1. *The approximating solution $\{U^n\}_{n=0}^{K_t}$ generated by ETD1 scheme (2.7) satisfies the energy inequality*

$$E_h(U^{n+1}) \leq E_h(U^n), \quad 0 \leq n \leq K_t - 1,$$

for any $\tau > 0$; i.e., the ETD1 scheme is unconditionally energy stable.

Proof. The difference between the discrete energies at two consecutive time levels yields

$$E_h(U^{n+1}) - E_h(U^n) = \frac{1}{4} \sum_{i=1}^{dN} [((U_i^{n+1})^2 - 1)^2 - ((U_i^n)^2 - 1)^2]$$

(5.1)
$$- \frac{\varepsilon^2}{2} [(U^{n+1})^T D_h U^{n+1} - (U^n)^T D_h U^n].$$

It is easy to verify that

$$\frac{1}{4}[(a^2 - 1)^2 - (b^2 - 1)^2] \le (b^3 - b)(a - b) + 2(a - b)^2 \qquad \forall \, a, b \in [-1, 1].$$

Since $\kappa \ge 2$, it follows from Theorem 3.4 that $\|U^n\|_\infty \le 1$ and $\|U^{n+1}\|_\infty \le 1$. Then we have

$$\frac{1}{4} \sum_{i=1}^{dN} [((U_i^{n+1})^2 - 1)^2 - ((U_i^n)^2 - 1)^2]$$
$$\le (U^{n+1} - U^n)^T ((U^n)^{.3} - U^n) + \kappa(U^{n+1} - U^n)^T (U^{n+1} - U^n)$$
$$= \kappa(U^{n+1} - U^n)^T U^{n+1} - (U^{n+1} - U^n)^T f(U^n).$$

On the other hand, direct calculations lead to

$$- \frac{\varepsilon^2}{2} [(U^{n+1})^T D_h U^{n+1} - (U^n)^T D_h U^n]$$
$$= -\varepsilon^2 (U^{n+1} - U^n)^T D_h U^{n+1} + \frac{\varepsilon^2}{2} (U^{n+1} - U^n)^T D_h (U^{n+1} - U^n)$$
$$\le -\varepsilon^2 (U^{n+1} - U^n)^T D_h U^{n+1}$$

due to the negative semidefiniteness of the matrix D_h. Thus, we obtain from (5.1) that

$$E_h(U^{n+1}) - E_h(U^n) \le \kappa(U^{n+1} - U^n)^T U^{n+1} - (U^{n+1} - U^n)^T f(U^n)$$
$$- \varepsilon^2 (U^{n+1} - U^n)^T D_h U^{n+1}$$
$$= (U^{n+1} - U^n)^T (L_h U^{n+1} - f(U^n)).$$

We solve $f(U^n)$ from (2.8), together with Lemma 2.2 (1), to get

$$f(U^n) = (I - e^{-L_h \tau})^{-1} L_h (U^{n+1} - e^{-L_h \tau} U^n)$$
$$= (I - e^{-L_h \tau})^{-1} L_h (U^{n+1} - U^n + (I - e^{-L_h \tau}) U^n)$$
$$= (I - e^{-L_h \tau})^{-1} L_h (U^{n+1} - U^n) + L_h U^n,$$

and then

$$L_h U^{n+1} - f(U^n) = L_h (U^{n+1} - U^n) - (I - e^{-L_h \tau})^{-1} L_h (U^{n+1} - U^n) = B_1 (U^{n+1} - U^n),$$

where $B_1 := L_h - (I - e^{-L_h \tau})^{-1} L_h$. Define a function

$$g_1(a) := a - \frac{a}{1 - e^{-a}}, \quad a \ne 0.$$

Then $g_1(a) < 0$ for any $a > 0$ and $B_1 = \tau^{-1} g_1(L_h \tau)$. Since L_h is symmetric and positive definite, by using Lemma 2.2 (2) and (3), we know that B_1 is symmetric and negative definite. Therefore, we obtain

$$E_h(U^{n+1}) - E_h(U^n) \le (U^{n+1} - U^n)^T B_1 (U^{n+1} - U^n) \le 0,$$

which completes the proof. □

For ETDRK2 scheme (2.9), we can prove the uniform boundedness of the discretized energy E_h.

THEOREM 5.2. *Under the assumptions of Theorem 4.2, the approximate solution $\{U^n\}_{n=0}^{K_t}$ generated by ETDRK2 scheme (2.9) satisfies*

$$E_h(U^{n+1}) \le E_h(U^n) + \widetilde{C} h^{-\frac{1}{2}} (h^2 + \tau)^2, \quad 0 \le n \le K_t - 1,$$

for any $h > 0$ and $0 < \tau \le 1$, where the constant $\widetilde{C}$ is independent of h and τ. Furthermore, if $h \le 1$ and $\tau = \lambda \sqrt{h}$ for some constant $\lambda > 0$, we have

$$E_h(U^n) \le E_h(U^0) + \widehat{C}, \quad 0 \le n \le K_t,$$

where the constant $\widehat{C}$ is independent of h and τ; i.e., the discrete energy is uniformly bounded.

Proof. The first step is to calculate the increment $E_h(U^{n+1}) - E_h(U^n)$ directly, which is completely identical to the proof for the ETD1 scheme, and we obtain

$$E_h(U^{n+1}) - E_h(U^n) \le (U^{n+1} - U^n)^T (L_h U^{n+1} - f(U^n)).$$

Using (2.10a) and (2.10b), we then get

$$(5.2) \qquad U^{n+1} = \phi_0(L_h \tau) U^n + \tau \phi_1(L_h \tau) f(U^n) + \tau \phi_2(L_h \tau)(f(\widetilde{U}^{n+1}) - f(U^n)).$$

Premultiplying $(\tau \phi_1(L_h \tau))^{-1}$ to both sides of (5.2) gives us

$$f(U^n) = (I - \mathrm{e}^{-L_h \tau})^{-1} L_h (U^{n+1} - U^n) + L_h U^n$$
$$- (L_h \tau)^{-1}(I - \mathrm{e}^{-L_h \tau})^{-1}(\mathrm{e}^{-L_h \tau} - I + L_h \tau)(f(\widetilde{U}^{n+1}) - f(U^n)),$$

and then, using the notation B_1 defined in the proof for the ETD1 scheme, we obtain

$$L_h U^{n+1} - f(U^n) = B_1 (U^{n+1} - U^n) + B_2 (f(\widetilde{U}^{n+1}) - f(U^n)),$$

where $B_2 = g_2(L_h \tau)$ with

$$g_2(a) := \frac{\mathrm{e}^{-a} - 1 + a}{a(1 - \mathrm{e}^{-a})}, \quad a \ne 0.$$

Since $0 < g_2(a) < 1$ for any $a > 0$, we know that B_2 is symmetric and positive definite and $\|B_2\|_2 < 1$. Using the mean-value theorem, we have

$$f(\widetilde{U}^{n+1}) - f(U^n) = G^n(\widetilde{U}^{n+1} - U^n),$$

where G^n is a diagonal matrix with, according to (3.2), diagonal entries between 0 and $\kappa + 1$, which implies that $\|G^n\|_\infty \le \kappa + 1$. Then, by the negative definiteness of B_1, we obtain

$$E_h(U^{n+1}) - E_h(U^n) \le (U^{n+1} - U^n)^T B_2 G^n(\widetilde{U}^{n+1} - U^n).$$

According to Theorem 4.2, we can derive

$$\|U^{n+1} - U^n\|_\infty \leq \|U^{n+1} - I^h u(t_{n+1})\|_\infty + \|I^h(u(t_{n+1}) - u(t_n))\|_\infty + \|I^h u(t_n) - U^n\|_\infty$$
$$\leq C_6 e^{t_{n+1}}(h^2 + \tau^2) + C_7 \tau + C_6 e^{t_n}(h^2 + \tau^2)$$
$$\leq C_8(h^2 + \tau)$$

for any $h > 0$ and $\tau \in (0, 1]$, where C_6 and C_7 depend on the $C^2([0, T]; C^4_{\text{per}}(\overline{\Omega}))$-norm of u and $C_8 = 2C_6 e^T + C_7$. Similarly, using Theorem 4.1, we can obtain

$$\|\widetilde{U}^{n+1} - U^n\|_\infty \leq C_9(h^2 + \tau),$$

with the constant $C_9 > 0$ depending on T and the $C^1([0, T]; C^4_{\text{per}}(\overline{\Omega}))$-norm of u. In addition, we have

$$\|B_2 G^n\|_\infty \leq \sqrt{dN}\|B_2\|_2\|G^n\|_\infty \leq \sqrt{dN}(\kappa + 1) = h^{-\frac{1}{2}}\sqrt{dX}(\kappa + 1).$$

Therefore, we obtain

$$E_h(U^{n+1}) - E_h(U^n) \leq \widetilde{C} h^{-\frac{1}{2}}(h^2 + \tau)^2,$$

where the constant $\widetilde{C} = C_8 C_9 \sqrt{dX}(\kappa + 1)$ is independent of h and τ. By induction, we further obtain

$$E_h(U^n) \leq E_h(U^0) + \widetilde{C} T h^{-\frac{1}{2}} \tau^{-1}(h^2 + \tau)^2, \quad 0 \leq n \leq K_t.$$

When $h \leq 1$ and $\tau = \lambda\sqrt{h}$, it holds that $h^{-\frac{1}{2}}\tau^{-1}(h^2 + \tau)^2 \leq (\lambda + 1)^2/\lambda$. The proof is then completed by setting $\widehat{C} = \widetilde{C} T(\lambda + 1)^2/\lambda$. □

6. Numerical experiments. In this section, we will carry out some numerical experiments in the 2D space to demonstrate the effectiveness and efficiency of the ETD schemes (2.7) and (2.9) for solving NAC equation (1.1). The fractional power kernel

$$(6.1) \qquad \rho_\delta(r) = \frac{2(4 - \alpha)}{\pi \delta^{4-\alpha} r^\alpha} \chi_{(0,\delta]}(r), \quad \alpha \in [0, 4),$$

is chosen and satisfies the finite second order moment condition (1.3). When $\alpha \in [0, 2)$, the kernel satisfies $\rho_\delta(|\boldsymbol{s}|) \in L^1(\mathbb{R}^2)$, which means that the nonlocal diffusion operator $\mathcal{L}_\delta$ is a bounded linear operator in this case. The kernel is nonintegrable when $\alpha \in [2, 4)$. We first verify the temporal and spatial convergence rates of the fully discrete schemes with a smooth initial data, and then we check the discrete maximum principle and energy stability of the evolutions beginning with a random initial state. Next, we present a further numerical investigation on the steady state solutions of the model with integrable kernels. ETDRK2 scheme (2.9) is adopted in all the simulations, while ETD1 scheme (2.7) is only considered for the temporal convergence tests due to the lack of high accuracy. The domain $\Omega = (0, 2\pi) \times (0, 2\pi)$ is used in all examples. We also take the stabilizing parameter $\kappa = 2$ for the numerical schemes in all experiments.

6.1. Convergence tests.

EXAMPLE 6.1. *We consider NAC equation* (1.1) *with smooth initial data* $u_0(x, y) = 0.5 \sin x \sin y$. *We set the interfacial parameter* $\varepsilon = 0.1$ *and the terminal time* $T = 0.5$. *For the kernel* (6.1), $\alpha = 1$ *(integrable) and* $\alpha = 3$ *(nonintegrable) are adopted, respectively.*

First, by setting $N = 256$, we tested the convergence in time for the cases $\delta = 0.2$ and $\delta = 2$. We calculated the numerical solutions of the NAC equation using ETD1 scheme (2.7) and ETDRK2 scheme (2.9) with various time step sizes $\tau = 0.05 \times 2^{-k}$ with $k = 0, 1, \ldots, 7$. To compute the errors, we treated the solution obtained by the ETDRK2 scheme with $\tau = 10^{-6}$ as the benchmark. The maximum norms of the numerical errors and corresponding convergence rates are given in Table 1, where the expected temporal convergence rates (1 for ETD1 and 2 for ETDRK2) are obviously observed in both cases of integrable and nonintegrable kernels. It is also easy to see that the numerical errors are almost independent of the choices of δ and α.

TABLE 1
Temporal convergence rates in the maximum-norm sense in Example 6.1.

$\tau = 0.05$	$\alpha = 1$ (integrable kernel)				$\alpha = 3$ (nonintegrable kernel)			
	$\delta = 0.2$		$\delta = 2$		$\delta = 0.2$		$\delta = 2$	
	Error	Rate	Error	Rate	Error	Rate	Error	Rate
ETD1								
τ	1.082e-2	–	1.090e-2	–	1.084e-2	–	1.087e-2	–
$\tau/2$	5.535e-3	0.967	5.580e-3	0.967	5.545e-3	0.967	5.561e-3	0.967
$\tau/4$	2.800e-3	0.983	2.823e-3	0.983	2.805e-3	0.983	2.813e-3	0.983
$\tau/8$	1.408e-3	0.992	1.420e-3	0.992	1.410e-3	0.992	1.415e-3	0.992
$\tau/16$	7.060e-4	0.996	7.121e-4	0.996	7.074e-4	0.996	7.095e-4	0.996
$\tau/32$	3.536e-4	0.998	3.566e-4	0.998	3.542e-4	0.998	3.553e-4	0.998
$\tau/64$	1.769e-4	0.999	1.784e-4	0.999	1.772e-4	0.999	1.778e-4	0.999
$\tau/128$	8.849e-5	1.000	8.924e-5	1.000	8.865e-5	1.000	8.892e-5	1.000
ETDRK2								
τ	6.410e-4	–	6.464e-4	–	6.422e-4	–	6.441e-4	–
$\tau/2$	1.676e-4	1.935	1.690e-4	1.935	1.679e-4	1.935	1.684e-4	1.935
$\tau/4$	4.287e-5	1.967	4.323e-5	1.967	4.294e-5	1.967	4.308e-5	1.967
$\tau/8$	1.084e-5	1.984	1.093e-5	1.984	1.086e-5	1.984	1.089e-5	1.984
$\tau/16$	2.726e-6	1.993	2.749e-6	1.992	2.730e-6	1.992	2.739e-6	1.992
$\tau/32$	6.834e-7	1.996	6.892e-7	1.996	6.846e-7	1.996	6.867e-7	1.996
$\tau/64$	1.711e-7	1.998	1.725e-7	1.998	1.714e-7	1.998	1.719e-7	1.998
$\tau/128$	4.278e-8	2.000	4.314e-8	2.000	4.285e-8	2.000	4.299e-8	2.000

Next, we tested the convergence with respect to the spatial size h by fixing $\delta = 2$ and $\tau = T$. The numerical solution of the NAC equation obtained by the ETDRK2 scheme with $N = 4096$ is treated as the benchmark for computing the errors of the numerical solutions obtained with $N = 2^k$ with $k = 4, 5, \ldots, 10$. The numerical errors in the maximum-norm sense are presented in Table 2. It is observed that the convergence rates with respect to h are almost of second order in both cases of integrable and nonintegrable kernels, which is again consistent with the theoretical results.

TABLE 2
Spatial convergence rates in the maximum-norm sense in Example 6.1.

$h = \dfrac{\pi}{8}$	$\alpha = 1$		$\alpha = 3$	
	Error	Rate	Error	Rate
h	1.554e-4	–	1.258e-4	–
$h/2$	2.430e-5	2.677	3.328e-5	1.918
$h/4$	4.491e-6	2.436	7.441e-6	2.161
$h/8$	8.679e-7	2.371	2.017e-6	1.883
$h/16$	2.068e-7	2.069	4.701e-7	2.101
$h/32$	4.944e-8	2.064	1.344e-7	1.807
$h/64$	6.590e-9	2.908	3.483e-8	1.948

We also investigated the limit behaviors of the numerical solutions of (1.1) as $\delta \to 0$. By fixing $N = 4096$ and $\tau = T$, we calculated the numerical solutions of the NAC equation obtained by ETDRK2 scheme (2.9) with various δ's and compared them with the numerical solution of the LAC equation. Table 3 collects the errors between the nonlocal and local numerical solutions in the maximum-norm sense, and the second order convergence with respect to δ is obviously observed.

TABLE 3

Rates of convergence to the local limits in the maximum-norm sense in Example 6.1.

$\delta = 0.2$	$\alpha = 1$		$\alpha = 3$	
	Error	Rate	Error	Rate
δ	1.076e-5	–	5.371e-6	–
$\delta/2$	2.703e-6	1.993	1.344e-6	1.999
$\delta/4$	6.250e-7	2.112	3.153e-7	2.091
$\delta/8$	1.580e-7	1.984	6.373e-8	2.307

6.2. Stability tests. For the case $\rho_\delta(|\boldsymbol{s}|) \in L^1(\mathbb{R}^2)$, i.e., $\alpha \in [0, 2)$, it has been proved in [15] that the steady state solution u^* of NAC equation (1.1) is continuous if $\varepsilon^2 C_\delta \geq 1$, where

$$C_\delta = \int_{B_\delta(\boldsymbol{0})} \rho_\delta(|\boldsymbol{s}|) \, \mathrm{d}\boldsymbol{s} = \frac{4(4 - \alpha)}{(2 - \alpha)\delta^2}.$$

Under certain assumptions, if $\varepsilon^2 C_\delta < 1$, the locally increasing u^* has a discontinuity at x_* with the jump

$$(6.2) \qquad \llbracket u^* \rrbracket(x_*) = 2\sqrt{1 - \varepsilon^2 C_\delta}.$$

EXAMPLE 6.2. *We simulate NAC equation* (1.1) *with a random initial data ranging from* -0.9 *to* 0.9 *uniformly generated on the* 512×512 *mesh. We set the interfacial parameter* $\varepsilon = 0.1$ *and adopt the kernel* (6.1) *with* $\alpha = 1$ *and various* δ's. *For comparison, we also simulate LAC equation* (1.5) *with the same settings. The time step is set to be* $\tau = 0.01$ *for all cases.*

Under these settings, the critical value of δ satisfying $\varepsilon^2 C_\delta = 1$ is $\delta_0 = 2\sqrt{3}\varepsilon$. The three rows in Figure 1 correspond to the evolutions of phase structures governed by the LAC equation and the NAC equations with $\delta = 3\varepsilon$ and $\delta = 4\varepsilon$ at times $t = 6, 14, 50$, and 180, respectively. Figure 2 presents the evolutions of the corresponding maximum norms and the energies of the numerical solutions, respectively. It is observed in all cases that the discrete maximum principle is preserved perfectly and the discrete energy decays monotonically. It is easy to see that the dynamics of the NAC equation with $\delta = 3\varepsilon$ is quite similar to that of the LAC equation. The evolution processes of these two cases reach the steady states at about $t = 190$ and $t = 370$, respectively, while the evolution of the NAC equation with $\delta = 4\varepsilon$ lasts much longer time. In addition, the NAC equation with $\delta = 3\varepsilon$ has a thinner and sharper interface than the LAC equation but a wider interface than the NAC equation equation with $\delta = 4\varepsilon$. Actually, the interface in the case $\delta = 4\varepsilon$ is discontinuous since the condition $\varepsilon^2 C_\delta < 1$ holds. The discontinuities in the solutions will be investigated further in the next example.

6.3. Discontinuity in the steady state solution.

EXAMPLE 6.3. *We simulate the evolution of a bubble governed by NAC equation* (1.1) *starting with a smooth initial configuration (see Figure* 3*). Again, we set the*
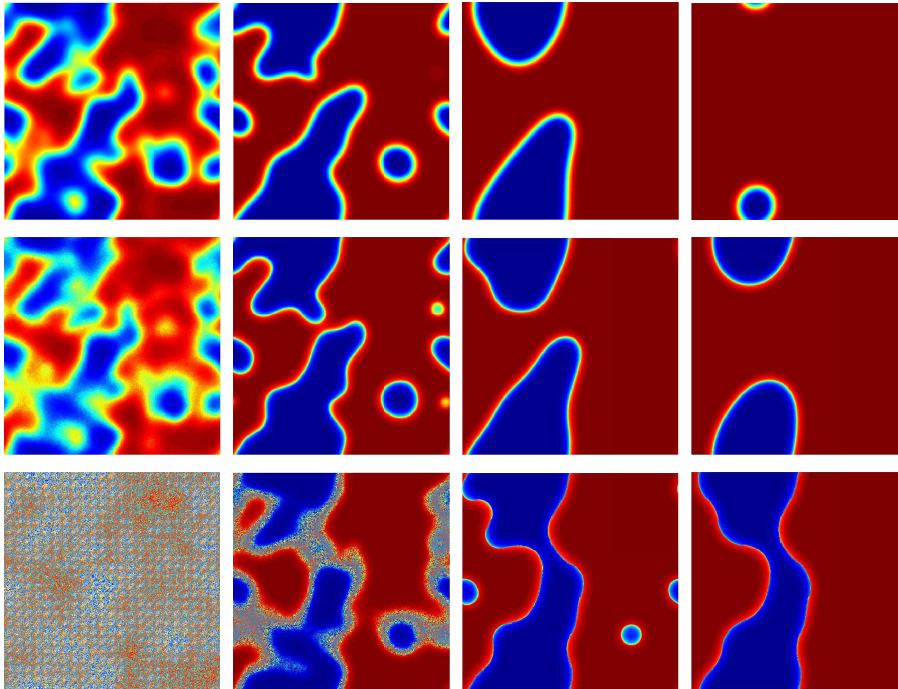
FIG. 1. *Evolutions of phase structures governed by the LAC equation (top row) and the NAC equations with $\delta = 3\varepsilon$ (middle row) and $\delta = 4\varepsilon$ (bottom row) in Example* 6.2. *From left to right: $t = 6, 14, 50, 180$.*
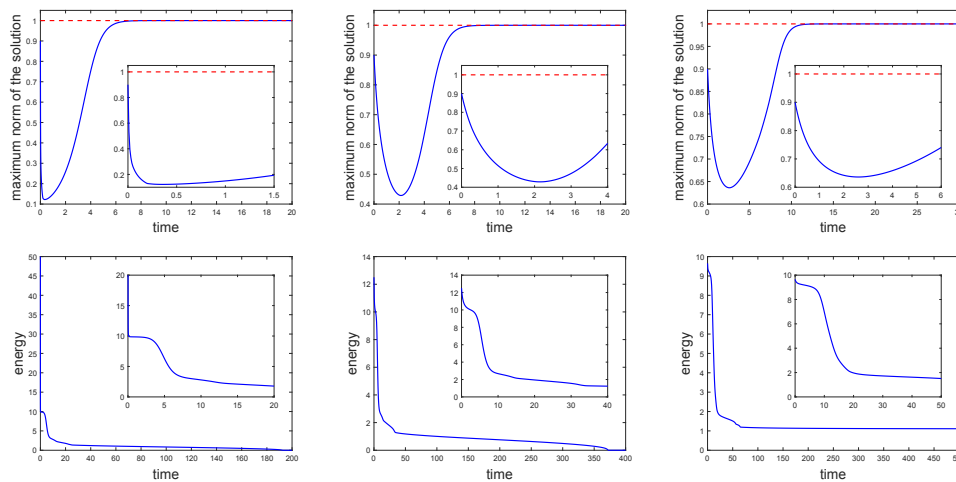

FIG. 2. *Evolutions of the maximum norms (top row) and the energies (bottom row) of the numerical solutions in Example* 6.2. *From left to right: governed by the LAC equation and the NAC equations with $\delta = 3\varepsilon$ and $\delta = 4\varepsilon$.*

interfacial parameter $\varepsilon = 0.1$ *and adopt the kernel* (6.1) *with $\alpha = 1$ and various δ's. The parameters of the space-time mesh are set to $\tau = 0.01$ and $N = 2048$ for all cases.*
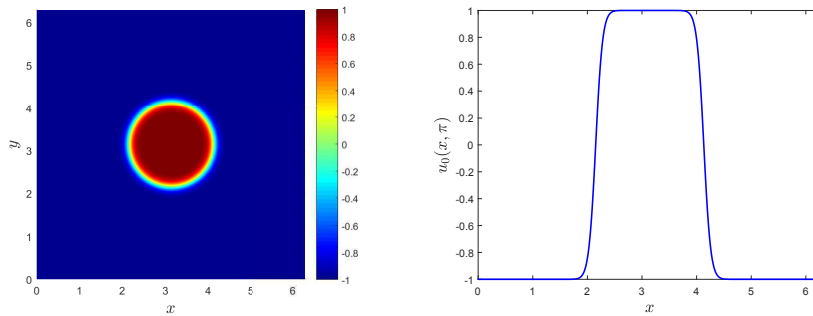
Fig. 3. *Initial configuration of Example* 6.3. *Left: surface-project view; right: cross-section view at* $y = \pi$.

This example is devoted to the relationship between the discontinuities in the steady state solutions and the horizon parameter δ. Under the settings of the parameters given above, it is known from (6.2) that the theoretical values of the jumps occurring at the discontinuity points can be formulated as

$$\text{Theoretical jump} = 2\sqrt{1 - \frac{0.12}{\delta^2}}, \quad \delta > \delta_0 = \sqrt{0.12} \approx 0.3464.$$

We chose several δ's ($\delta = 0.8, 1.6, 3.2$) larger than δ_0 to observe the discontinuities and the jumps in the numerical results, and for the comparison we also considered one case ($\delta = 0.2$) with δ smaller than the critical value. Table 4 collects the theoretical and numerically computed jumps occurring at the discontinuity points in the steady state solutions with various δ's. It is observed that the numerical jumps match the theoretical values very well.

TABLE 4
Theoretical and numerical jumps in steady state solutions in Example 6.3.

	$\delta = 0.2$	$\delta = 0.8$	$\delta = 1.6$	$\delta = 3.2$
Theoretical jumps	0	1.802776	1.952562	1.988247
Numerical jumps	0	1.804496	1.952713	1.988242

Figure 4 presents the evolutions of the bubble governed by the NAC equations with $\delta = 0.2$ ($< \delta_0$), $\delta = 0.8$, and $\delta = 3.2$ (both $> \delta_0$), respectively. In each row, the first three graphs give the surface-projection views of the numerical solutions at several times and the last graph cross-section views with $y = \pi$ by zooming in around the interface. For the case $\delta = 0.2$, the bubble shrinks quickly and finally disappears, which is similar to the process of the shrinkage occurring in the case of the LAC equation (see [8]). The evolutions for cases $\delta = 0.8$ and $\delta = 3.2$ are similar: the bubble does not shrink and the interface turns sharper and sharper so that the solution preforms discontinuity on the interface after some times and reaches the steady state with the expected jump. It is seen from this example that the NAC equation with small δ has more similar dynamics to the local model, which is consistent with the observations in Example 6.2, while the NAC equation with large δ, especially larger than δ_0, leads to the steady state solution within the discontinuity even though the initial state is smooth.
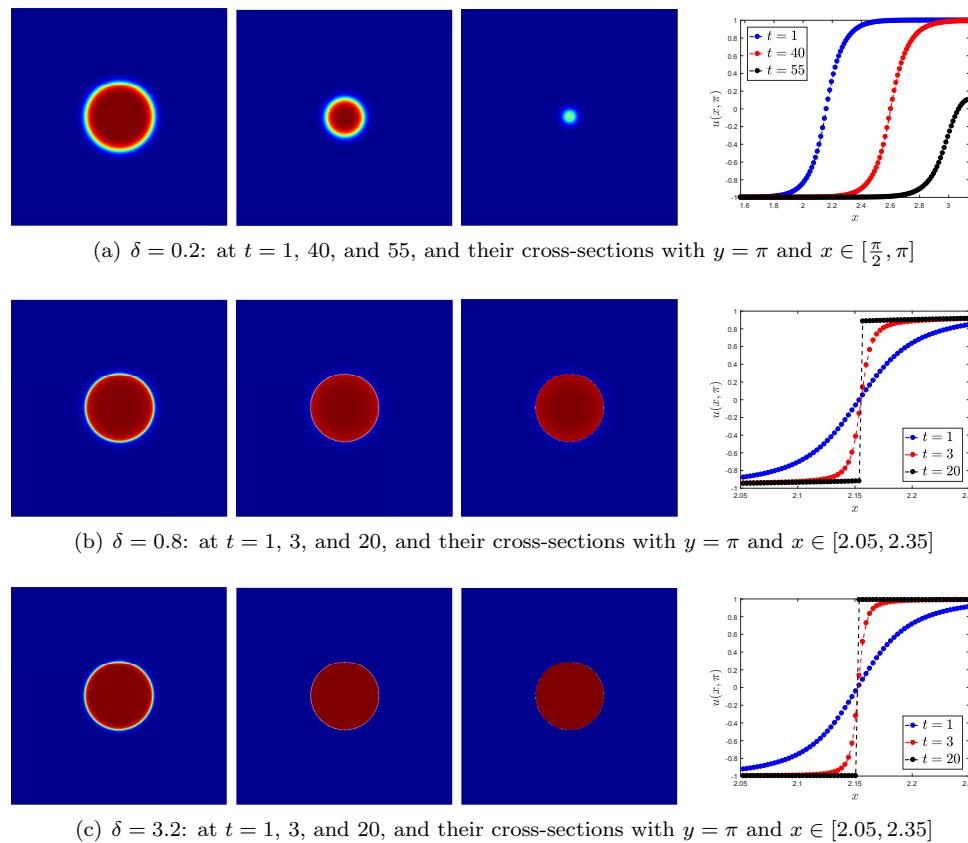
(a) $\delta = 0.2$: at $t = 1$, 40, and 55, and their cross-sections with $y = \pi$ and $x \in \left[\frac{\pi}{2}, \pi\right]$

(b) $\delta = 0.8$: at $t = 1$, 3, and 20, and their cross-sections with $y = \pi$ and $x \in [2.05, 2.35]$

(c) $\delta = 3.2$: at $t = 1$, 3, and 20, and their cross-sections with $y = \pi$ and $x \in [2.05, 2.35]$

FIG. 4. *Evolutions of the bubble governed by the NAC equations with $\delta = 0.2, 0.8, 3.2$ in Example* 6.3.

7. Conclusion. We designed and analyzed maximum principle preserving numerical schemes for solving the nonlocal Allen–Cahn equation by using the quadrature-based finite difference method for spatial discretizations and the exponential time differencing method for temporal integrations. Especially, we developed the first order ETD and second order ETD Runge–Kutta schemes, derived the error estimates for both schemes, and proved their energy stability along with the asymptotic compatibility, a special convergence considered for the numerical approximations of nonlocal models. Numerical experiments were carried out to verify the theoretical results and to study some more interesting properties of the solutions caused by the nonlocality. The maximum principle preserving schemes studied here are up to the second order in time. Whether higher order numerical schemes can preserve the maximum principle still remains open and is the subject of one of our future works. In addition, for some other models, for instance, the nonlocal Cahn–Hilliard equation [13, 22], the solution does not possess the maximum principle but is L^∞ stable instead. Numerical schemes naturally inheriting the L^∞ stability, weaker than the maximum principle, are also worthy of study.

REFERENCES

[1] S. M. ALLEN AND J. W. CAHN, *A microscopic theory for antiphase boundary motion and its application to antiphase domain coarsening*, Acta Metall., 27 (1979), pp. 1085–1095.

[2] S. ARMSTRONG, S. BROWN, AND J. L. HAN, *Numerical analysis for a nonlocal phase field system*, Int. J. Numer. Anal. Model. Ser. B, 1 (2010), pp. 1–9.

[3] F. ANDREU, J. M. MAZON, J. D. ROSSI, AND J. TOLEDO, *Nonlocal Diffusion Problems*, Math. Surveys Monogr. 165, AMS, Providence, RI, 2010.

[4] P. W. BATES, *On some nonlocal evolution equations arising in materials science*, Fields Inst. Commun., 48 (2006), pp. 13–52.

[5] P. W. BATES, S. BROWN, AND J. L. HAN, *Numerical analysis for a nonlocal Allen–Cahn equation*, Int. J. Numer. Anal. Model., 6 (2009), pp. 33–49.

[6] G. BEYLKIN, J. M. KEISER, AND L. VOZOVOI, *A new class of time discretization schemes for the solution of nonlinear PDEs*, J. Comput. Phys., 147 (1998), pp. 362–387.

[7] F. BOBARU AND M. DUANGPANYA, *The peridynamic formulation for transient heat conduction*, Internat. J. Heat Mass Transfer, 53 (2010), pp. 4047–4059.

[8] L. Q. CHEN AND J. SHEN, *Applications of semi-implicit Fourier-spectral method to phase-field equations*, Comput. Phys. Comm., 108 (1998), pp. 147–158.

[9] S. M. COX AND P. C. MATTHEWS, *Exponential time differencing for stiff systems*, J. Comput. Phys., 176 (2002), pp. 430–455.

[10] Q. DU, *Nonlocal Modeling, Analysis, and Applications*, CBMS-NSF Res. Conf. Ser. in Appl. Math. 94, SIAM, Philadelphia, 2019, https://doi.org/10.1137/1.9781611975628.

[11] Q. DU, M. GUNZBURGER, R. B. LEHOUCQ, AND K. ZHOU, *Analysis and approximation of nonlocal diffusion problems with volume constraints*, SIAM Rev., 54 (2012), pp. 667–696, https://doi.org/10.1137/110833294.

[12] Q. DU, M. GUNZBURGER, R. B. LEHOUCQ, AND K. ZHOU, *A nonlocal vector calculus, nonlocal volume-constrained problems, and nonlocal balance laws*, Math. Models Methods Appl. Sci., 23 (2013), pp. 493–540.

[13] Q. DU, L. JU, X. LI, AND Z. H. QIAO, *Stabilized linear semi-implicit schemes for the nonlocal Cahn–Hilliard equation*, J. Comput. Phys., 363 (2018), pp. 39–54.

[14] Q. DU, Y. Z. TAO, X. C. TIAN, AND J. YANG, *Asymptotically compatible discretization of multidimensional nonlocal diffusion models and approximation of nonlocal Greens functions*, IMA J. Numer. Anal., (2018), dry011, https://doi.org/10.1093/imanum/dry011.

[15] Q. DU AND J. YANG, *Asymptotically compatible Fourier spectral approximations of nonlocal Allen–Cahn equations*, SIAM J. Numer. Anal., 54 (2016), pp. 1899–1919, https://doi.org/10.1137/15M1039857.

[16] Q. DU AND K. ZHOU, *Mathematical analysis for the peridynamic nonlocal continuum theory*, Math. Model. Numer. Anal., 45 (2011), pp. 217–234.

[17] Q. DU AND W.-X. ZHU, *Stability analysis and application of the exponential time differencing schemes*, J. Comput. Math., 22 (2004), pp. 200–209.

[18] Q. DU AND W.-X. ZHU, *Analysis and applications of the exponential time differencing schemes and their contour integration modifications*, BIT, 45 (2005), pp. 307–328.

[19] P. C. FIFE, *Some nonclassical trends in parabolic and parabolic-like evolutions*, in Trends in Nonlinear Analysis, Springer, Berlin, 2003, pp. 153–191.

[20] H. GAJEWSKI AND K. GÄRTNER, *On a nonlocal model of image segmentation*, Z. Angew. Math. Phys., 56 (2005), pp. 572–591.

[21] G. GILBOA AND S. OSHER, *Nonlocal operators with applications to image processing*, Multiscale Model. Simul., 7 (2008), pp. 1005–1028, https://doi.org/10.1137/070698592.

[22] Z. GUAN, C. WANG, AND S. M. WISE, *A convergent convex splitting scheme for the periodic nonlocal Cahn–Hilliard equation*, Numer. Math., 128 (2014), pp. 377–406.

[23] N. J. HIGHAM, *Functions of Matrices: Theory and Computation*, SIAM, Philadelphia, 2008, https://doi.org/10.1137/1.9780898717778.

[24] M. HOCHBRUCK AND A. OSTERMANN, *Explicit exponential Runge–Kutta methods for semilinear parabolic problems*, SIAM J. Numer. Anal., 43 (2005), pp. 1069–1090, https://doi.org/10.1137/040611434.

[25] M. HOCHBRUCK AND A. OSTERMANN, *Exponential integrators*, Acta Numer., 19 (2010), pp. 209–286.

[26] T. L. HOU, T. TANG, AND J. YANG, *Numerical analysis of fully discretized Crank–Nicolson scheme for fractional-in-space Allen–Cahn equations*, J. Sci. Comput., 72 (2017), pp. 1214–1231.

[27] L. JU, X. LI, Z. H. QIAO, AND H. ZHANG, *Energy stability and error estimates of exponential time differencing schemes for the epitaxial growth model without slope selection*, Math. Comp., 87 (2018), pp. 1859–1885.

[28] L. Ju, J. Zhang, and Q. Du, *Fast and accurate algorithms for simulating coarsening dynamics of Cahn–Hilliard equations*, Comput. Mater. Sci., 108 (2015), pp. 272–282.

[29] L. Ju, J. Zhang, L. Y. Zhu, and Q. Du, *Fast explicit integration factor methods for semilinear parabolic equations*, J. Sci. Comput., 62 (2015), pp. 431–455.

[30] A. C. Lazer, *Characteristic exponents and diagonally dominant linear differential systems*, J. Math. Anal. Appl., 35 (1971), pp. 215–229.

[31] B. Li and J.-G. Liu, *Thin film epitaxy with or without slope selection*, European J. Appl. Math., 14 (2003), pp. 713–743.

[32] D. Li and Z. H. Qiao, *On second order semi-implicit Fourier spectral methods for 2D Cahn-Hilliard equations*, J. Sci. Comput., 70 (2017), pp. 301–341.

[33] D. Li, Z. H. Qiao, and T. Tang, *Characterizing the stabilization size for semi-implicit Fourier-spectral method to phase field equations*, SIAM J. Numer. Anal., 54 (2016), pp. 1653–1681, https://doi.org/10.1137/140993193.

[34] Z. H. Qiao and S. Y. Sun, *Two-phase fluid simulation using a diffuse interface model with Peng–Robinson equation of state*, SIAM J. Sci. Comput., 36 (2014), pp. B708–B728, https://doi.org/10.1137/130933745.

[35] J. Shen, T. Tang, and J. Yang, *On the maximum principle preserving schemes for the generalized Allen–Cahn equation*, Commun. Math. Sci., 14 (2016), pp. 1517–1534.

[36] J. Shen and X. F. Yang, *Numerical approximations of Allen–Cahn and Cahn–Hilliard equations*, Discrete Contin. Dyn. Syst., 28 (2010), pp. 1669–1691.

[37] S. A. Silling, *Reformulation of elasticity theory for discontinuities and long-range forces*, J. Mech. Phys. Solids, 48 (2000), pp. 175–209.

[38] S. A. Silling and R. B. Lehoucq, *Peridynamic theory of solid mechanics*, Adv. Appl. Mech., 44 (2010), pp. 73–168.

[39] T. Tang and J. Yang, *Implicit-explicit scheme for the Allen–Cahn equation preserves the maximum principle*, J. Comput. Math., 34 (2016), pp. 471–481.

[40] Y. Z. Tao, X. C. Tian, and Q. Du, *Nonlocal diffusion and peridynamic models with Neumann type constraints and their numerical approximations*, Appl. Math. Comput., 305 (2017), pp. 282–298.

[41] H. Tian, L. Ju, and Q. Du, *A conservative nonlocal convection-diffusion model and asymptotically compatible finite difference discretization*, Comput. Methods Appl. Mech. Engrg., 320 (2017), pp. 46–67.

[42] X. C. Tian and Q. Du, *Analysis and comparison of different approximations to nonlocal diffusion and linear peridynamic equations*, SIAM J. Numer. Anal., 51 (2013), pp. 3458–3482, https://doi.org/10.1137/13091631X.

[43] X. C. Tian and Q. Du, *Asymptotically compatible schemes and applications to robust discretization of nonlocal models*, SIAM J. Numer. Anal., 52 (2014), pp. 1641–1665, https://doi.org/10.1137/130942644.

[44] X. Q. Wang, L. Ju, and Q. Du, *Efficient and stable exponential time differencing Runge–Kutta methods for phase field elastic bending energy models*, J. Comput. Phys., 316 (2016), pp. 21–38.

[45] S. M. Wise, C. Wang, and J. S. Lowengrub, *An energy-stable and convergent finite-difference scheme for the phase field crystal equation*, SIAM J. Numer. Anal., 47 (2009), pp. 2269–2288, https://doi.org/10.1137/080738143.

[46] C. J. Xu and T. Tang, *Stability analysis of large time-stepping methods for epitaxial growth models*, SIAM J. Numer. Anal., 44 (2006), pp. 1759–1779, https://doi.org/10.1137/050628143.

[47] X. F. Yang, *Linear, first and second-order, unconditionally energy stable numerical schemes for the phase field model of homopolymer blends*, J. Comput. Phys., 327 (2016), pp. 294–316.

[48] X. F. Yang and D. Z. Han, *Linearly first- and second-order, unconditionally energy stable schemes for the phase field crystal model*, J. Comput. Phys., 330 (2017), pp. 1116–1134.

[49] J. Zhang, C. B. Zhou, Y. G. Wang, L. Ju, Q. Du, X. B. Chi, D. S. Xu, D. X. Chen, Y. Liu, and Z. Liu, *Extreme-scale phase field simulations of coarsening dynamics on the Sunway Taihulight supercomputer*, in Proceedings of the International Conference for High Performance Computing, Networking, Storage and Analysis (SC'16), IEEE Press, 2016, 4.

[50] K. Zhou and Q. Du, *Mathematical and numerical analysis of linear peridynamic models with nonlocal boundary conditions*, SIAM J. Numer. Anal., 48 (2010), pp. 1759–1780, https://doi.org/10.1137/090781267.

[51] L. Y. Zhu, L. Ju, and W. D. Zhao, *Fast high-order compact exponential time differencing Runge–Kutta methods for second-order semilinear parabolic equations*, J. Sci. Comput., 67 (2016), pp. 1043–1065.